
A FRAMEWORK FOR ANALYZING CROSS-CORRELATORS USING PRICE'S THEOREM AND PIECEWISE-LINEAR DECOMPOSITION

Zhili Xiao

Electrical & Systems Engineering
Washington University in Saint Louis
Saint Louis, MO 63130
xiaozhili@wustl.edu

Shantanu Chakrabartty

Electrical & Systems Engineering
Washington University in Saint Louis
Saint Louis, MO 63130
shantanu@wustl.edu

ABSTRACT

Precise estimation of cross-correlation or similarity between two random variables lies at the heart of signal detection, hyperdimensional computing, associative memories, and neural networks. Although a vast literature exists on different methods for estimating cross-correlations, the question *what is the best and the simplest method to estimate cross-correlations using finite samples?* is still unclear. In this paper, we first argue that the standard empirical approach might not be optimal, even though the estimator exhibits uniform convergence to the true cross-correlation. Instead, we show that there exists a large class of simple non-linear functions that can be used to construct cross-correlators with a higher signal-to-noise ratio (SNR). To demonstrate this, we first present a general mathematical framework using Price's Theorem that allows us to analyze arbitrary cross-correlators constructed using a mixture of piece-wise linear functions. Using this framework and a high-dimensional mapping, we show that some of the most promising cross-correlators are based on Huber's loss functions, margin-propagation (MP) functions, and the log-sum-exponential (LSE) functions.

1 Introduction

Estimating cross-correlations between random variables play an important role in the field of statistics [1], machine learning [2, 3, 4, 5], and signal detection [6, 7, 8, 9]. This is because the cross-correlation metric measures some form of similarity between the random variables, revealing how one might influence the other. With proper normalization, the metric becomes equivalent to cosine similarity and unitary transforms, both of which are extensively used in linear algebra [10], natural language processing [11], and computer vision [12, 13]. In computer vision and signal processing, cross-correlation is often used for feature extraction [14], where higher precision implies more information is retained for further data processing and learning. Accurate and efficient cross-correlation for pattern recognition and template matching [15, 16] also ensures reliable and real-time decision-making in applications like radar detection or object recognition. In the emerging field of hyperdimensional computing [17, 18], cross-correlations (or equivalently inner-products) are used for information retrieval from sparse distributed memories [19, 20]. Since most of the vectors in higher-dimensions are nearly orthogonal to each other, precision in cross-correlation is essential to discriminate between patterns and improve the robustness of learning [21, 22].

In its most general form, cross-correlation $R : \mathbb{R} \times \mathbb{R} \rightarrow \mathbb{R}$ is defined for a pair of random variables $X \in \mathbb{R}$, $Y \in \mathbb{R}$ as

$$R := \mathcal{E}[XY] = \int_{-\infty}^{\infty} \int_{-\infty}^{\infty} xy p(X = x, Y = y) dx dy, \quad (1)$$

where $p : \mathbb{R} \times \mathbb{R} \rightarrow \mathbb{R}^+$ denotes the underlying joint probability distribution from which x and y are drawn from. The operator $\mathcal{E}[\cdot]$ denotes an expectation under the probability measure p .

In practice, the joint distribution p is not known a priori. Instead, one has access to N samples independently drawn from the distribution p , as illustrated in Fig. 1c. If we denote the sample vectors as $\mathbf{x} \in \mathbb{R}^N$ and $\mathbf{y} \in \mathbb{R}^N$, then the

All correspondences related to this manuscript should be addressed to shantanu@wustl.edu.

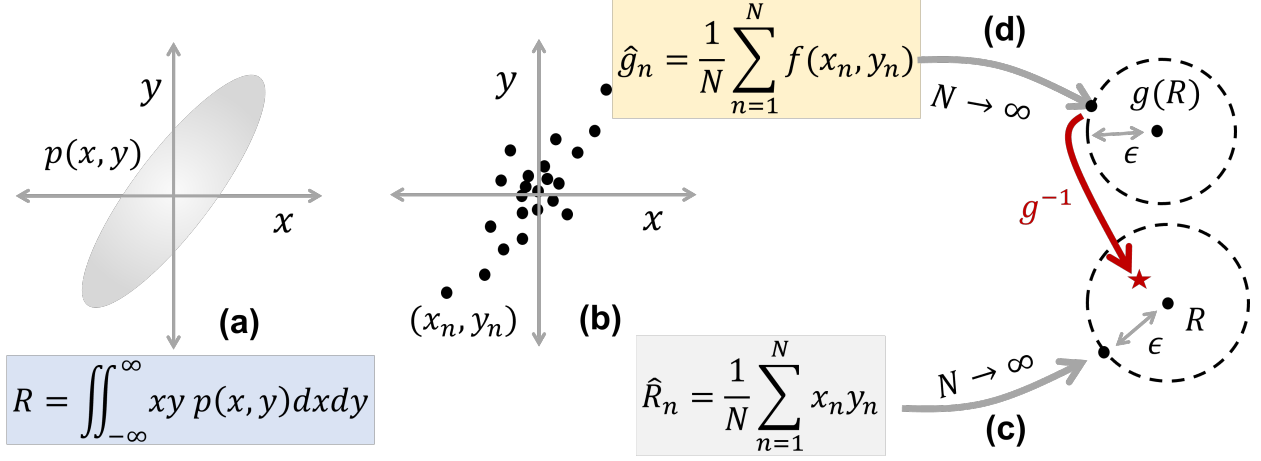


Figure 1: (a) Statistical definition of cross-correlation R between random variables x and y under a joint distribution $p(x, y)$; (b) Empirical cross-correlation \hat{R}_N based on samples (x_n, y_n) ; (c) Uniform convergence of \hat{R}_N to R ; (d) Uniform convergence of empirical non-linear cross-correlator \hat{g}_N to $g(R)$; and (e) Estimation of R using g^{-1} .

cross-correlation is empirically estimated as

$$\hat{R}_N = \frac{1}{N} \sum_{n=1}^N x_n y_n, \quad (2)$$

where $x_n \in \mathbb{R}$ and $y_n \in \mathbb{R}$ represent the elements of the vector \mathbf{x} and \mathbf{y} . Then, by the law of large numbers (LLN), the empirical correlation converges uniformly to the true correlation R

$$\left| \frac{1}{N} \sum_{n=1}^N x_n y_n - R \right| \leq \epsilon \xrightarrow{N \rightarrow \infty} 0, \quad (3)$$

as depicted in Fig. 1.

In this paper, we refer to the above estimation approach using multiplication of samples as the empirical approach, and we explore an alternate approach towards estimating cross-correlations using a class of non-linear functions of samples $f : \mathbb{R} \times \mathbb{R} \rightarrow \mathbb{R}$ such that

$$\frac{1}{N} \sum_{n=1}^N f(x_n, y_n) \xrightarrow{N \rightarrow \infty} \mathcal{E}[f(X, Y)] = g(R), \quad (4)$$

where $g : \mathbb{R} \rightarrow \mathbb{R}$ is a monotonic function.

The uniform convergence of f is illustrated in Fig. 1 where

$$\left| \frac{1}{N} \sum_{n=1}^N f(x_n, y_n) - g(R) \right| \leq \epsilon \xrightarrow{N \rightarrow \infty} 0. \quad (5)$$

The main premise of this paper is that when x and y are drawn from a stationary distribution, the function g is known apriori or can be estimated with high accuracy. As a result, for a finite sample size N , $g^{-1}(\frac{1}{N} \sum_{n=1}^N f(x_n, y_n))$ is an unbiased cross-correlation estimator, and its estimation could be closer than \hat{R} to the true cross-correlation R , as illustrated in Fig. 1d.

For the analysis and comparison presented in this paper, we will assume the following without loss of generality.

1. Both the random variables X and Y for which the cross-correlation is being estimated will be assumed to be zero mean $\mathcal{E}[X] = \mathcal{E}[Y] = 0$ and have unit variance $\mathcal{E}[X^2] = \mathcal{E}[Y^2] = 1$. In this case, the cross-correlation R is equal to Pearson's correlation coefficient [23]. Note that if X, Y have nonzero means μ_x and μ_y , the cross-correlation can be expressed as follow,

$$\mathcal{E}[XY] = \mathcal{E}[(X - \mu_x)(Y - \mu_y)] + \mu_x \mu_y. \quad (6)$$

Since $\mu_x \mu_y$ can be determined apriori, the accuracy of different cross-correlators is determined by the accuracy of the cross-correlation between the zero mean variables $X' = X - \mu_x$ and $Y' = Y - \mu_y$.

2. The non-linear function $f(x, y)$ used for generating different cross-correlators is passive and memory-less which implies that its output depends on the instantaneous values of X and Y .

The paper is organized as follows: In section 2, we first propose the mathematical framework that can be used to analyze cross-correlators for a general class of non-linear function f and for jointly Gaussian distributed inputs. We use the framework to analyze different types of estimators, which include the linear-rectifier cross-correlator, margin-propagation (MP) cross-correlators [24], Huber-type [25] cross-correlators, and log-sum-exponential (LSE) [26] estimators. In section 3, we extend the framework to arbitrary input distributions based on the hyperdimensional mapping using the Walsh-Hadamard transformation. In section 4, we show experiments evaluating different correlators and the transformation method. Section 5 discusses the advantages and disadvantages of different correlators and concludes the paper with a brief perspective on future directions.

2 Analysis Framework using Price's Theorem

In this section, we present an analytical framework that can be used to understand the behavior of different cross-correlators. A cross-correlator can be viewed as a difference between two functions, and in Fig. 2(a), we illustrate this for the empirical cross-correlator defined in equation (2), which can be expressed as

$$\frac{1}{N} \sum_{n=1}^N x_n y_n = \frac{1}{4N} \sum_{n=1}^N (x_n + y_n)^2 - (x_n - y_n)^2. \quad (7)$$

The symmetric quadratic functions $(x + y)^2$ and $-(x - y)^2$ are shown in Fig. 2a, which results in the product xy when summed together. When extended to N dimensions, the quadratic functions in equation (2) become L_2 distances $\|\mathbf{x} + \mathbf{y}\|_2^2$ and $\|\mathbf{x} - \mathbf{y}\|_2^2$ and their difference is proportional to the empirical cross-correlation $\frac{1}{N} \sum_{n=1}^N x_n y_n$. The concept can be generalized to other norms [27]. As an example, it has been suggested that substituting the quadratic component with linear rectifiers can yield a comparable cross-correlator [28, 29] which uses L_1 distances $|\mathbf{x} + \mathbf{y}|$ and $|\mathbf{x} - \mathbf{y}|$. Typically, the linear rectifier cross-correlator is considered a reasonable approximation of the empirical cross-correlator. In Fig. 2b, we show the equivalent construction for the L_1 type cross-correlators using L_1 distances $|\mathbf{x} + \mathbf{y}|$ and $|\mathbf{x} - \mathbf{y}|$.

Both L_2 and L_1 constructions can be viewed as special cases of mixtures of piece-wise linear functions as shown in Fig. 2c and can be expressed as

$$f(x, y) = h(x + y) - h(x - y), \quad (8)$$

where

$$h(x) = \frac{1}{2} \sum_{l=1}^L w_l (|x - \alpha_l| + |x + \alpha_l|), \quad (9)$$

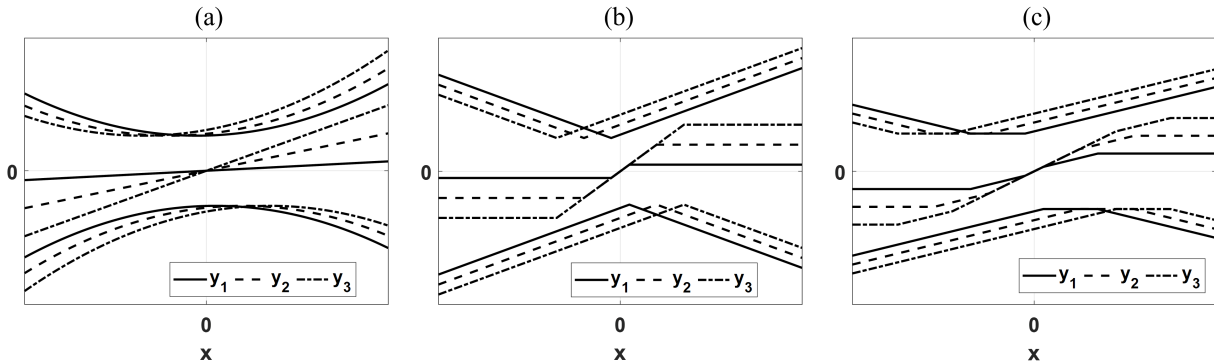


Figure 2: A conceptual scalar demonstration of a) empirical correlators, b) L_1 type correlators, and c) an example of correlators using mixtures of piece-wise linear functions with $L = 1$, $w_1 = 1$, and $\alpha_1 = 0.5$. All correlators $f(x, y)$ can be viewed as a difference between $h(x + y)$ and $h(x - y)$. The upper three curves represent $h(x + y)$, the lower three curves represent $-h(x + y)$, and curves in the middle are $f(x, y)$ for different values of $y = y_1, y_2, y_3$.

with parameters $\alpha_l \geq 0, w_l \geq 0; \sum_l w_l = 1$ and $|\cdot|$ is an absolute-value function defined as

$$|x| = \begin{cases} x & ; x \geq 0 \\ -x & ; x < 0. \end{cases} \quad (10)$$

We now state the Lemma that can be used to compute the function $g(R) = \mathcal{E}[f(x, y)]$.

Lemma 2.1. *If the function $f(x, y)$ is given by equation (8) and (9) and the joint probability distribution of $X \in \mathbb{R}$ and $Y \in \mathbb{R}$ is given by*

$$p(X = x, Y = y; R) = \frac{1}{2\pi\sqrt{1-R^2}} \exp\left[-\frac{x^2 + y^2 - 2Rxy}{2(1-R^2)}\right], \quad (11)$$

where $R \in [-1, 1]$ is the Pearson's correlation/cross-correlation between x and y , then $g(R) = \mathcal{E}[f(X, Y)]$ is given by

$$g(R) = \frac{1}{2\sqrt{\pi}} \sum_{l=1}^L \int_0^R \frac{w_l}{\sqrt{(1+\rho)}} \exp\left[-\frac{\alpha_l^2}{4(1+\rho)}\right] + \frac{w_l}{\sqrt{(1-\rho)}} \exp\left[-\frac{\alpha_l^2}{4(1-\rho)}\right] d\rho. \quad (12)$$

Proof. Since f is a memory-less function with a well-defined Fourier transform and X and Y are zero-mean, unit variance, jointly distributed Gaussian random variables, we can apply Price's theorem [30, 29, 31] which states that

$$\frac{\partial \mathcal{E}(f)}{\partial R} = \mathcal{E}\left[\frac{\partial^2 f}{\partial x \partial y}\right], \quad (13)$$

where the expectation operator \mathcal{E} is defined as

$$\mathcal{E}(f) = \int_{-\infty}^{\infty} \int_{-\infty}^{\infty} f(x, y) p(x, y; R) dx dy = g(R). \quad (14)$$

The partial derivatives of the sub-functions $h(x+y), h(x-y)$ in (9) are

$$\frac{\partial^2 h(x+y)}{\partial x \partial y} = \frac{1}{2} \sum_{l=1}^L w_l [\delta(x+y-\alpha_l) + \delta(x+y+\alpha_l)], \quad (15a)$$

$$-\frac{\partial^2 h(x-y)}{\partial x \partial y} = \frac{1}{2} \sum_{l=1}^L w_l [\delta(x-y-\alpha_l) + \delta(x-y+\alpha_l)], \quad (15b)$$

where $\delta(\cdot)$ denotes the Dirac-delta function. The expectation operators can be computed as follow

$$\begin{aligned} \mathcal{E}\left[\frac{\partial^2 h(x+y)}{\partial x \partial y}\right] &= \frac{1}{2} \sum_{l=1}^L w_l \int_{-\infty}^{\infty} p(x, -x+\alpha_l) + p(x, -x-\alpha_l) dx \\ &= \frac{1}{\sqrt{\pi(1+R)}} \sum_{l=1}^L w_l \exp\left[-\frac{\alpha_l^2}{4(1+R)}\right] \end{aligned} \quad (16a)$$

$$\begin{aligned} -\mathcal{E}\left[\frac{\partial^2 h(x-y)}{\partial x \partial y}\right] &= \frac{1}{2} \sum_{l=1}^L w_l \int_{-\infty}^{\infty} p(x, x-\alpha_l) + p(x, x+\alpha_l) dx \\ &= \frac{1}{\sqrt{\pi(1-R)}} \sum_{l=1}^L w_l \exp\left[-\frac{\alpha_l^2}{4(1-R)}\right]. \end{aligned} \quad (16b)$$

Substituting the results into (8) and (13) will get

$$\frac{\partial g}{\partial R} = \frac{1}{\sqrt{\pi(1+R)}} \sum_{l=1}^L w_l \exp\left[-\frac{\alpha_l^2}{4(1+R)}\right] + \frac{1}{\sqrt{\pi(1-R)}} \sum_{l=1}^L w_l \exp\left[-\frac{\alpha_l^2}{4(1-R)}\right], \quad (17)$$

which leads to the expression for $g(R)$,

$$g(R) = \int_0^R \frac{1}{\sqrt{\pi(1+\rho)}} \sum_{l=1}^L w_l \exp\left[-\frac{\alpha_l^2}{4(1+\rho)}\right] d\rho + \int_0^R \frac{1}{\sqrt{\pi(1-\rho)}} \sum_{l=1}^L w_l \exp\left[-\frac{\alpha_l^2}{4(1-\rho)}\right] d\rho. \quad (18)$$

□

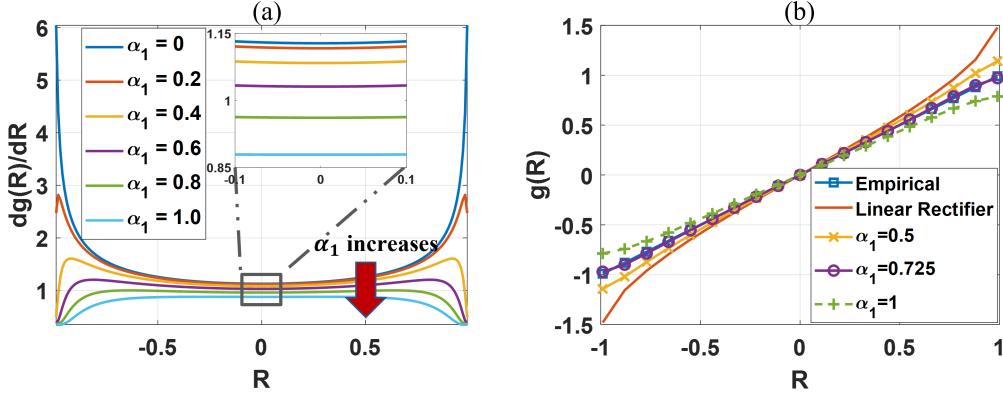


Figure 3: a): $\frac{\partial g}{\partial R}$ for $L = 1, w_1 = 1$, and $\alpha_1 = \{0, 0.2, 0.4, 0.6, 0.8, 1.0\}$; b) The $g(R)$ of the empirical and linear rectifier correlators and the $g(R)$ derived by integrating $\frac{\partial g}{\partial R}$ for $L = 1, w_1 = 1$, and $\alpha_1 = 0.5, 0.725$ and 1 . It demonstrates how the analysis framework can be used to construct varying correlators with different output characteristics.

Example 1: When $L = 1, w_1 = 1, \alpha_1 = 0$, the function f is reduced to

$$f(x, y) = |x + y| - |x - y|, \quad (19)$$

which is the well-studied linear rectifier correlator. In this case, the relation (12) can be evaluated in closed form and is given by

$$g_{L1}(R) = \frac{2}{\sqrt{\pi}}(\sqrt{1+R} - \sqrt{1-R}). \quad (20)$$

Example 2: When $w_l = 1/L, \alpha_l = c/L, l = 1, \dots, L$ and $c, L \rightarrow \infty$, the function f is reduced to

$$f(x, y) = \frac{1}{2c}((x+y)^2 - (x-y)^2), \quad (21)$$

where $c > |x|$ is the range of inputs. So the function f becomes the empirical correlator. In this case, the summation in the relation (12) can be replaced by integrals in the limit $L \rightarrow \infty$ in which case

$$\frac{\partial g_{L2}}{\partial R} = \frac{1}{c\sqrt{\pi(1+R)}} \int_0^\infty \exp\left[-\frac{x^2}{4(1+R)}\right] dx + \frac{1}{c\sqrt{\pi(1-R)}} \int_0^\infty \exp\left[-\frac{x^2}{4(1-R)}\right] dx = \frac{2}{c}. \quad (22)$$

Therefore, $g_{L2}(R) = \frac{2}{c}R$ matches the result for a scaled empirical cross-correlation.

The above examples show how specific cross-correlators can be constructed using Lemma 2.1. Even though the equation (12) may not be solved in closed-form, it is analytical and hence can be used to visualize the form of $g(R)$ for specific choices of α_l and w_l . Fig. 3a visualizes the partial derivative $\frac{\partial g}{\partial R}$ in (17) when $L = 1, w_1 = 1$, and $\alpha_1 = \{0, 0.2, 0.4, 0.6, 0.8, 1\}$. The zoomed-in window demonstrates that the partial derivatives stay almost constant around zero correlation, which implies the linearity of $g(R)$ around zero correlation for any cross-correlators. Fig. 3b displays the $g(R)$ of both empirical and linear rectifier correlators and the $g(R)$ for different values of a single offset $\alpha_1 = 0.5, 0.725, 1$ computed by integration. The results will be verified by the Monte Carlo experiment for MP correlators in section 4.

Let's denote $\mathcal{E}(f)$ or $g(R)$ by y , we can derive the following from $g_{L1}(R)$ in (20)

$$R^2 = \frac{\pi}{4}y^2 - \frac{\pi^2}{64}y^4. \quad (23)$$

This suggests that g^{-1} in Fig. 1 can be robustly estimated using a polynomial expansion with a relatively low degree. This is important since the closed-form solution for equation (18) may not be computed for different choices of w_l, α_l . As a result, g^{-1} has to be learned/estimated by drawing samples with known apriori cross-correlation, which is then used to estimate R according to Fig. 1. As we will show later in section 3, this calibration procedure and procedure to estimate R can be agnostic to the input distribution.

We now apply the calibration procedure to three other types of functions of the type given by expression (8). The first is the margin-propagation (MP) function given by

$$(x - z)_+ + (-x - z)_+ = \gamma, \quad (24)$$

$$h(x) = z, \quad (25)$$

where $(\cdot)_+$ is the ReLU function, and $\gamma \geq 0$ is the hyper-parameter. It can be easily verified that the MP function in (24) is equivalent to (9) with $L = 1$ and $\alpha_1 = 0.5\gamma$.

The second function is the Huber function which requires an infinite number of splines and is given by

$$h(x) = \begin{cases} 0.5x^2/\delta, & x < \delta \\ |x| - \frac{1}{2}\delta, & x \geq \delta, \end{cases} \quad (26)$$

where $\delta > 0$ is a threshold parameter.

The third function is a log-sum-exp (LSE) function which also requires an infinite number of splines and is given by

$$h(x) = \frac{1}{a}(\log(\exp[ax] + \exp[-ax])), \quad (27)$$

where $a > 0$ is a scaling factor.

As we will show in section 4, the Huber and LSE correlators fall between the empirical and linear rectifier correlators, hence the inverse cross-correlation function g^{-1} can be approximated by a polynomial of degree lower or equal to the degree needed for g_{L1}^{-1} . In practice, we found that fourth order polynomial is sufficient for calibration of g_{L1}^{-1} . For calibrating MP correlators, higher degree polynomials were needed as the value of γ increases as its $|\frac{\partial g}{\partial R}|$ is not monotonically increasing as correlation increases. As such, a fifth-order polynomial was used to learn the inverse cross-correlation function g^{-1} .

3 Extension to non-Gaussian distributions

The theoretical results presented in section 2 assumed random variables with joint Gaussian distributions. In this section, we extend the previous results for non-Gaussian distributions. To achieve this, we use results from the hyperdimensional computing literature, which state that variances and cross-correlations are preserved when random variables are mapped into high-dimensional space using unitary random matrices.

Lemma 3.1. *Let X and Y be zero-mean random variables with unit variance and with a cross-correlation R . Let $\Phi : \mathbb{R}^N \rightarrow \mathbb{R}^M$ denote a high-dimensional embedding using a Unitary transform such that $\mathcal{E}[\Phi(\mathbf{x})] = \mathbf{0}$. Then, as $N \rightarrow \infty$, $\frac{1}{N} \langle \Phi(\mathbf{x}), \Phi(\mathbf{y}) \rangle \rightarrow R$, where $\langle \cdot, \cdot \rangle$ is the inner product.*

Proof. Suppose \mathbf{x} and \mathbf{y} are \mathbb{R}^N -valued random vector, and each entry x_n, y_n are independently identically distributed (i.i.d) variables with the joint probability density function $p(X = x_n, Y = y_n; R)$

$$\frac{1}{N} \langle \Phi(\mathbf{x}), \Phi(\mathbf{y}) \rangle = \frac{1}{N} \langle \mathbf{x}, \mathbf{y} \rangle = \frac{1}{N} \sum_{n=1}^N x_n y_n \xrightarrow{N \rightarrow \infty} R. \quad (28)$$

□

The Walsh-Hadamard-Transform is one such unitary transform $\mathcal{H} : \mathbb{R}^N \rightarrow \mathbb{R}^N$ and it can be represented by a $N \times N$ Hadamard matrix. The transformation generally requires the input zero-padded to a power of two. An example 4×4 WHT matrix is shown below

$$H_4 = \frac{1}{2} \begin{pmatrix} 1 & 1 & 1 & 1 \\ 1 & -1 & 1 & -1 \\ 1 & 1 & -1 & -1 \\ 1 & -1 & -1 & 1 \end{pmatrix}. \quad (29)$$

The Hadamard matrices are orthogonal and symmetric matrices composed of +1 and -1 with a normalization factor $1/\sqrt{N}$, which makes it easy for implementations and computations. Besides keeping the covariance between random variables, it can also be shown that the transformed zero-mean variables converge to the joint Gaussian distribution with the same variance and covariance.

Lemma 3.2. *Let X and Y be zero-mean random variables with finite variances and the cross-correlation R . Let $\mathcal{H} : \mathbb{R}^N \rightarrow \mathbb{R}^N$ denote the Walsh-Hadamard-Transform. Suppose the entries of the vector equation $\mathbf{x}' = \mathcal{H}(\mathbf{x})$ are given by $x'_n = h_n(x_1, \dots, x_n)$, and $h_n(\cdot)$ is therefore*

$$h_n(x_1, \dots, x_n) = \begin{cases} \frac{1}{\sqrt{N}} \sum_{n=1}^N x_n, & n = 1, \\ \frac{1}{\sqrt{N}} (\sum_{n=1}^{N/2} x_n - \sum_{n=N/2+1}^N x_n), & n \neq 1, \end{cases} \quad (30)$$

where the x_n are independently identically distributed (i.i.d.) samples from X . Then, as $N \rightarrow \infty$, the joint probability distribution $p(x'_n, y'_n)$ converges to a bivariate Gaussian distribution with zero-mean, same variances σ_x^2, σ_y^2 , and covariance R .

Proof. Suppose X and Y are zero-mean random variables with finite variances and covariance R . According to the multivariate Central Limit Theorem (CLT) [32], as $N \rightarrow \infty$ the joint distribution $p(\sqrt{N}\bar{x}_N, \sqrt{N}\bar{y}_N)$ converges to bivariate Gaussian distribution with zero mean and the same variances and covariance R , where $\bar{x}_N = \frac{1}{N} \sum_{n=1}^N x_n$ is the average of N independently identically distributed samples of X .

Notice that the transformed entry after WHT $x'_n = h_n(x_1, \dots, x_n)$ can be expressed as

$$x'_n = \begin{cases} \sqrt{N}\bar{x}_N, & n = 1, \\ \frac{1}{\sqrt{2}} \sqrt{\frac{N}{2}} (\bar{x}_{N/2} - \bar{y}_{N/2}), & n \neq 1. \end{cases} \quad (31)$$

For $n = 1$, the CLT can be applied to the transformed input x'_1 and y'_1 . For the case of $n \neq 1$, note that the CLT also applies to $\pm \sqrt{\frac{N}{2}}\bar{x}_{N/2}$ and $\pm \sqrt{\frac{N}{2}}\bar{y}_{N/2}$, so they become bivariate Gaussian with zero means, and same variances and covariance, and so is their sum divided by $\sqrt{2}$. \square

As such, using the proof in section 2, it can be shown that for correlators that can be expressed by equations (8) and (9), the expected output $\mathcal{E}[f(\mathcal{H}(\mathbf{x}), \mathcal{H}(\mathbf{y}))]$ is equal to $g(R)$. In other words, for non-Gaussian distributed variables with zeros mean and finite covariance R , we can first transform the inputs to jointly Gaussian distribution, which preserves the covariance, and then use the cross-correlator in section 2 to estimate the cross-correlation R using the transformed data and the same g^{-1} .

4 Experiments Results and Analysis

In the first part of the experiments, we validate the analytical results in section 2 when the random variables are drawn from joint Gaussian distribution. For this specific case, a closed-form expression of the Cramér–Rao bound can be computed. This bound can then be used to evaluate the effectiveness of any unbiased cross-correlation estimators. We will then validate our analytical results for arbitrary input distributions.

4.1 Cross-correlation Cramér–Rao bound

According to the Cramér–Rao bound (CRB) [33], the variance or standard deviation of any unbiased estimator (satisfying regularity conditions) is lower bounded by the reciprocal of the Fisher information [34]. The following lemma presents the Cramér–Rao bound of the correlation estimator under the standard bivariate normal distribution.

Lemma 4.1. *For a collection of N independent and identically distributed (iid) bivariate variables $X \in \mathbb{R}$ and $Y \in \mathbb{R}$ drawn from the jointly Gaussian distribution defined by (11) the Cramér–Rao bound of the correlation estimator is given by*

$$\sigma^2(\hat{R}) \geq \frac{(1 - R^2)^2}{N(1 + R^2)}. \quad (32)$$

Proof. For the distribution (11), the Fisher information for the correlation coefficient of a single pair of samples (x, y) can be computed as,

$$I(R) = -\mathcal{E} \left[\frac{\partial^2 (l(x, y; R))}{\partial R^2} \right], \quad (33)$$

where $l(x, y; R)$ represents the natural logarithm likelihood function of a single sample pair (x, y) for the joint density function $p(X = x, Y = y; R)$

$$l(x, y; R) = -\log(2\pi) - \log(\sqrt{1 - R^2}) - \frac{x^2 + y^2 - 2Rxy}{2(1 - R^2)}. \quad (34)$$

From (34) and using $\mathcal{E}[X^2] = \mathcal{E}[Y^2] = 1$ and $\mathcal{E}[XY] = R$ leads to the Fisher's information metric

$$I(R) = \frac{1 + R^2}{(1 - R^2)^2}. \quad (35)$$

For N independent and identically distributed (iid) samples, the total Fisher information is the sum of information from each individual sample. Therefore, the Cramér–Rao bound is given by

$$\sigma^2(\hat{R}) \geq \frac{1}{I(R)} = \frac{(1 - R^2)^2}{N(1 + R^2)}. \quad (36)$$

□

In other words, the accuracy of all cross-correlators is upper bounded by the Fisher information. In section 4, we use the standard deviation of estimation errors σ to assess the performance of cross-correlators.

4.2 Monte-Carlo Experiments for Jointly Gaussian Inputs

This section presents the results using different correlators to estimate the covariance for standard jointly normal distribution. To study and compare their performance, vectors of different lengths are randomly sampled from the zero mean and unit variance Gaussian distribution. Each vector pair $\mathbf{s}_1, \mathbf{s}_2 \in \mathbb{R}^N$ is mixed in the following way to generate a bivariate Gaussian distribution $\mathbf{x} = (\mathbf{x}_1, \mathbf{x}_2)$ with different correlation R to learn and test the inverse cross-correlation function $g(R)$,

$$\mathbf{x}_1 = \mathbf{s}_1, \quad (37)$$

$$\mathbf{x}_2 = R\mathbf{s}_1 + \sqrt{1 - R^2}\mathbf{s}_2, \quad (38)$$

$$\mathbf{x} = (\mathbf{x}_1, \mathbf{x}_2) \sim \mathcal{N}(\tilde{\mathbf{0}}, \Sigma), \Sigma = \begin{pmatrix} 1 & R \\ R & 1 \end{pmatrix}. \quad (39)$$

Fig. 4 shows the average output of cross-correlation function $\hat{g}(R)$ corresponding to the MP, Huber, and LSE functions with different parameters, which is used as an approximation of the correlation function $g(R)$ to get the calibration function g^{-1} . The output of the empirical correlator is shown for comparison. Note that the linear rectifier correlator is a special case for the MP, Huber, and LSE functions, which is included and labeled as "MP $\gamma = 0$," "Huber $\delta = 0$," and "LSE $a \rightarrow \infty$." In fact, the normalized $g(R)$ for the Huber function and LSE functions are bounded above and below by the normalized $g_{L1}(R)$ and $g_{L2}(R)$. This is easy to see for Huber functions, as it's a combination of the quadratic

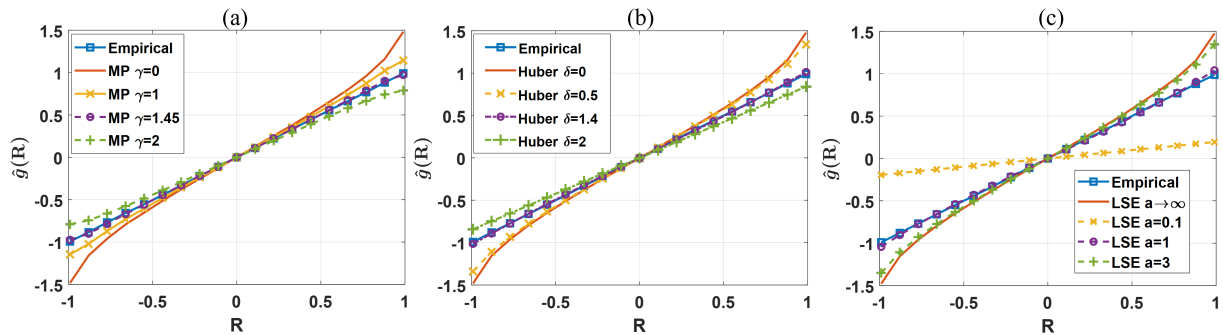


Figure 4: The estimated $\hat{g}(R)$ for the MP, Huber, and LSE functions for the standard bivariate normal distribution from Monte Carlo experiments. The expected outputs of the empirical and linear rectifier correlators are added for comparison. (a) The $\hat{g}(R)$ of MP correlators with $\gamma = \{0, 1, 1.45, 2\}$; (b) The $\hat{g}(R)$ of Huber correlators with $\delta = \{0.5, 1.4, 2\}$; (c) The $\hat{g}(R)$ of LSE correlators with $a = \{0.1, 1, 3\}$.

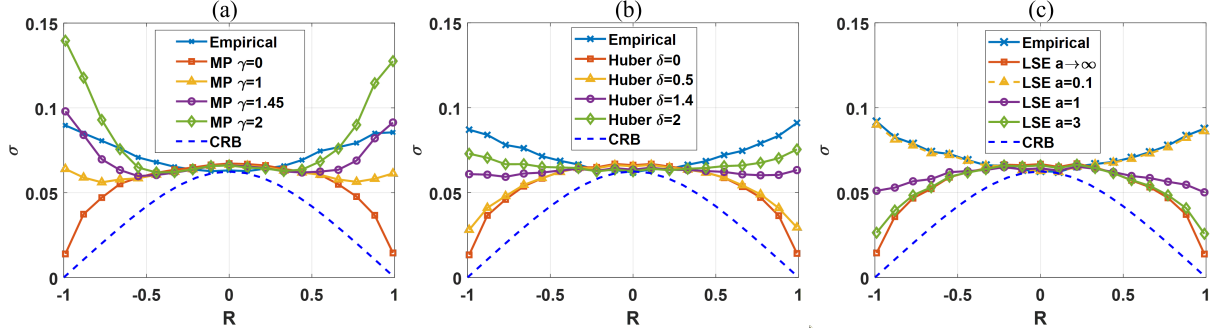


Figure 5: The standard deviation of the cross-correlation estimation error of MP, Huber, and LSE correlators for different correlation levels and the CRB at the dimension of 256, with the SNR of empirical and linear rectifier added for reference. (a) The error plot of MP correlators with $\gamma = \{1, 1.45, 2\}$; (b) The error plot of Huber correlators with $\sigma = \{0.5, 1.4, 2\}$; (c) The error plot of LSE correlators with $a = \{0.1, 1, 3\}$.

function (L_2) and absolute value function (L_1). For LSE functions, as the scaling factor a increases, the $h(x)$ for LSE functions in expression (27) can be simplified to $\frac{1}{a} \log(\exp[a|x|]) = |x|$ as the negative part will go to zero exponentially fast. On the other hand, as a decreases, we can Taylor expand the exponential function at zero, which leads to

$$h(x) = \frac{1}{a} \log\left(\sum_{n=0}^{\infty} \frac{(ax)^n}{n!} + \frac{(-ax)^n}{n!}\right). \quad (40)$$

The odd-degree terms cancel each other out and higher-order terms decay fast, which leads to

$$h(x) \approx \frac{1}{a} \log(2 + (ax)^2). \quad (41)$$

Applying the same trick to the logarithm but expanding at 2, we have

$$h(x) \approx \frac{1}{a} (\log(2) + \frac{1}{2}(ax)^2 + \dots) \approx \frac{1}{a} + \frac{1}{2}ax^2. \quad (42)$$

Therefore, the LSE correlator approaches the empirical correlator as a decreases.

As discussed in section 4.1, the standard deviation of estimation can be used to evaluate the performance of correlators. Since the expected value of g^{-1} is equal to R , the standard deviation of estimation $\sigma(\bar{R})$ is equivalent to the standard deviation of estimation error $\sigma(R - g^{-1}(f))$. In Fig. 5, we display the standard deviation of cross-correlation estimation errors and its CRB lower bound, denoted by σ , made by the MP, Huber, and LSE correlators with different parameters at different levels of cross-correlation using the learned inverse cross-correlation function g^{-1} . It is observed that the linear rectifier correlator is more accurate when the signal of interest is highly correlated, while the empirical correlator makes less error in the other case. The error profile of the Huber and LSE correlators becomes more similar to the

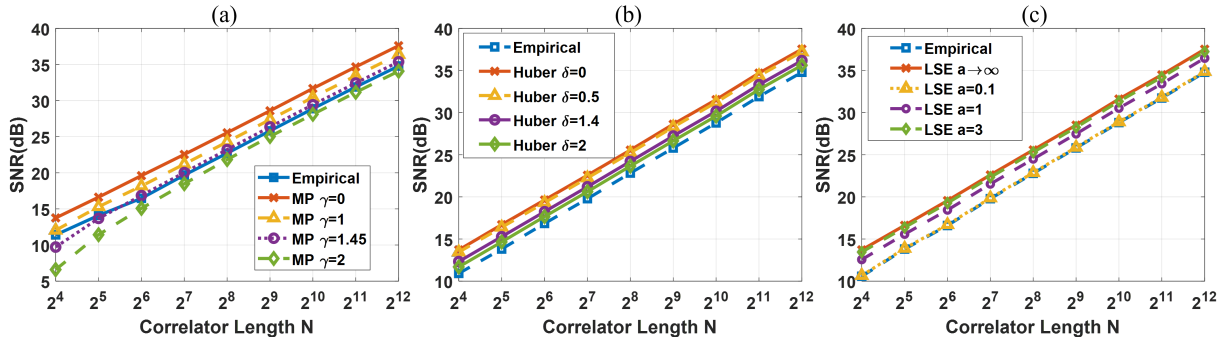


Figure 6: The SNR plots of MP, Huber, and LSE correlators from correlator length of 16 to 65536, with the SNR of empirical and linear rectifier correlators as a reference. a) The SNR plot of MP correlators with $\gamma = \{1, 1.45, 2\}$; b) The SNR plot of Huber correlators with $\sigma = \{0.5, 1.4, 2\}$; c) The SNR plot of LSE correlators with $a = \{0.1, 1, 3\}$.

empirical correlator when σ is high and a is small and approaches the linear rectifier correlator otherwise. The MP correlator in (24) is equivalent to the linear rectifier correlator when $\gamma = 0$. As γ increases, the performance degrades and performs even worse than the empirical correlator.

In Fig. 6, we plot the signal-to-noise-ratio (SNR) for these cross-correlators for different correlator length N , where the SNR is defined as:

$$\text{SNR} = 20 \log_{10} \left(\frac{1}{\bar{\sigma}} \right), \quad (43)$$

where $\bar{\sigma}$ is the average standard deviation of the error across multiple Monte-Carlo runs. The result shows that the linear rectifier correlator has the best SNR in joint Gaussian input distribution. Also, the SNR increases by 3dB when the correlation length N is doubled, which can be attributed to the reduction in the estimation error due to simple averaging.

4.3 Monte-Carlo Experiments with WHT and Non-Gaussian Inputs

In this section, the WHT method in section 3 was tested on non-Gaussian distributions to verify that the function $g(R)$ remains unchanged for non-Gaussian inputs after being transformed by the WHT. Fig. 7 shows varying joint input distributions before and after the WHT, which are denoted by blue crosses and red circles, respectively. The non-Gaussian distributions before the transformation are combinations of the uniform, Gaussian, and gamma distributions, and the inputs have a correlation of 0.8. It can be seen that the vectors become jointly Gaussian distributed after the transformation, and their correlation is retained. Monte-Carlo experiments show that the expected correlator output $\mathcal{E}[f(\mathcal{H}(x), \mathcal{H}(y))]$ is the same as the $g(R)$ for jointly Gaussian inputs. So no calibration is needed to learn g^{-1} for different distributions.

On the other hand, it should be noticed that the standard deviation for different cross-correlation estimators is not guaranteed to be the same for different input distributions, even after the WHT transformation. To see this, notice that the WHT process will not change the output for the empirical correlator because the WHT transformation is unitary. However, the standard deviation of the empirical correlator, which is given by

$$\mathcal{E}(XY - \mathcal{E}[XY])^2 = \mathcal{E}[X^2Y^2] - g^2(R) = \int_{-\infty}^{\infty} \int_{-\infty}^{\infty} x^2y^2 p(x,y) dx dy - g^2(R), \quad (44)$$

will change as the joint probability density function $p(x,y)$ changes. In particular, for joint Gaussian distribution, it can be verified that $\mathcal{E}(xy - \mathcal{E}[xy])^2 = 1 - R^2$, whereas it is $1 - \frac{1}{5}R^2$ in the case of jointly uniform distribution. As an example, Fig. 8 shows the standard deviation of estimation error plots for the joint uniform distribution as shown in Fig. 7a. It is observed that the contour of the error plot changes for all correlators except for the linear rectifier correlator, which is still the best-performing cross-correlation estimator in this specific non-Gaussian input distribution.

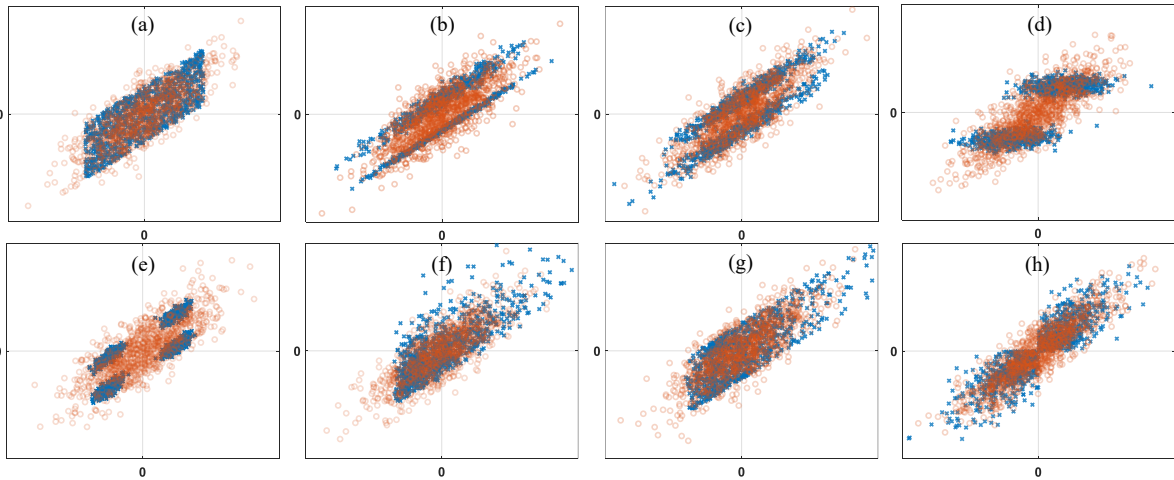


Figure 7: Scatter plots showing the random variables x and y drawn from different probability distributions with zero-mean, unit variance and a correlation $R=0.8$. The data points denoted by the blue cross are drawn from the original distribution and the data points denoted by the red circles are the inputs after applying WHT. After applying WHT, the resulting distribution converges towards a standard bivariate normal distribution with a correlation $R=0.8$.

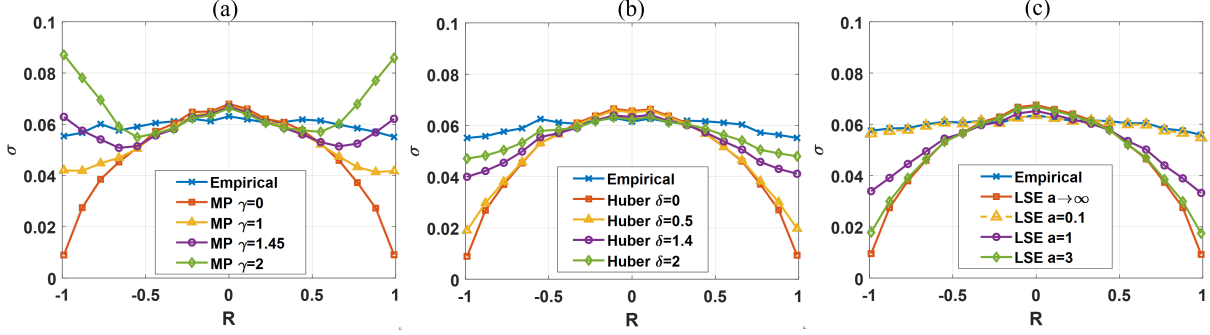


Figure 8: The standard deviation error plot of MP, Huber, and LSE correlators for the symmetric input distribution test when dimension is 256. a) The error plot of MP correlators with $\gamma = \{1, 1.45, 2\}$; b) The error plot of Huber correlators with $\sigma = \{0.5, 1.4, 2\}$; c) The error plot of LSE correlators with $a = \{0.1, 1, 3\}$.

5 Discussions and Conclusions

In this paper, we present a mathematical framework for analyzing different types of cross-correlators. The closed-form solution facilitates the comparison of different cross-correlators and allows us to understand performance trade-offs. The analysis framework has been verified by Monte Carlo simulation for different input distributions. The error analysis reveals that the shape of the error profile exhibits a trade-off. Cross-correlation estimators that exhibit high errors near $R \approx 0$ make fewer errors near $|R| \approx 1$. The hyperparameters of the Huber estimators, MP estimators, and LSE estimators can be adapted to achieve different error profiles.

However, the complexity of implementing these different online estimators on hardware could be significantly different. The empirical and Huber cross-correlator relies on the quadratic function and hence may be difficult to implement on hardware. On the other hand, the MP and LSE correlators can be easily implemented on analog hardware [35]. Another benefit of employing other correlators is the potential for improved computational efficiency and wider dynamic range when implementing them on digital systems. It is evident that the linear rectifier correlator and the MP correlator (without additional offsets) are more cost-effective than the empirical correlator since each multiplication is replaced by three and five addition operations [36]. The computation of the linear rectifier can be further simplified to condition and shift operations, and the addition operation is resistant to underflow on a fixed-point system. Moreover, the LSE correlator exhibits superior numerical stability at the expense of computational complexity, a common technique employed in machine learning to address the issue of gradient updates.

If an accurate estimate of the covariance or Pearson's correlation is necessary, then the calibration is required to learn the inverse function g^{-1} for inputs with diverse distributions and variances. To this end, the WHT is proposed as a pre-processing technique to convert input distributions to joint normal distributions, allowing the calibration process to be indifferent to input distributions. The limitation is that the transformation requires the dimension of inputs to be a power of two. However, calibration is still needed for varying variances, which inevitably introduces extra computational and resource expenses. On the other hand, the raw correlator output $f(\cdot)$ would be sufficient if the objective of the task is to obtain only a similarity score for different signals. For instance, in hyperdimensional computing, whether some $y \in \mathbb{R}^N$ is contained in a set $\mathcal{S} \in \mathbb{R}^N$ is checked by if the dot product $\langle \phi(y), \phi(\mathcal{S}) \rangle$ is above a certain threshold, where $\phi(\cdot)$ is the hyperdimensional representation. The WHT can be incorporated into the hyperdimensional mapping process ϕ , and alternative correlation functions, such as those discussed, can be used instead of resource-intensive and computationally inefficient inner products.

Regarding the accuracy for estimating the cross-correlation of jointly Gaussian distributed inputs, it appears that the empirical method may not be the most effective correlator. The linear rectifier correlator is superior in estimating the covariance for highly correlated signals and in terms of overall SNR. Its standard deviation of error plot has a similar trend with the Cramér–Rao bound (CRB). The performance gained for high correlation can be explained by the shape of $g(R)$. The variance of output $f(x, y)$ is relatively small with respect to the gradient of $g(R)$ for high correlation, which results in a larger confidence interval for estimations. The Huber and LSE correlator's performance is bounded by the linear rectifier and empirical correlator. The MP correlator in (24) is equivalent to the linear rectifier correlator when $\gamma = 0$. As γ increases, its performance for higher γ values can be potentially improved by introducing offsets. Of course, the above observations are not guaranteed to hold for other input distributions and are left for future research.

References

- [1] D.S. Moore, G.P. McCabe, and B.A. Craig. *Introduction to the Practice of Statistics*. W. H. Freeman, 2014.
- [2] Y. Lecun, L. Bottou, Y. Bengio, and P. Haffner. Gradient-based learning applied to document recognition. *Proceedings of the IEEE*, 86(11):2278–2324, 1998.
- [3] K.I. Diamantaras and Sun-Yuan Kung. Cross-correlation neural network models. *IEEE Transactions on Signal Processing*, 42(11):3218–3223, 1994.
- [4] M. Betke and N.C. Makris. Fast object recognition in noisy images using simulated annealing. In *Proceedings of IEEE International Conference on Computer Vision*, pages 523–530, 1995.
- [5] Richard O. Duda and Peter E. Hart. Pattern classification and scene analysis. In *A Wiley-Interscience publication*, 1974.
- [6] Jae-Chern Yoo and Tae Hee Han. Fast normalized cross-correlation. *Circuits, systems and signal processing*, 28:819–843, 2009.
- [7] S. Adrián-Martínez, M. Ardid, M. Bou-Cabo, I. Felis, C. Llorens, J. A. Martínez-Mora, and M. Saldaña. Acoustic signal detection through the cross-correlation method in experiments with different signal to noise ratio and reverberation conditions, 2015.
- [8] Hsueh-Jyh Li, Yung-Deh Wang, and Long-Huai Wang. Matching score properties between range profiles of high-resolution radar targets. *IEEE Transactions on Antennas and Propagation*, 44(4):444–452, 1996.
- [9] H.-J. Li and S.-H. Yang. Using range profiles as feature vectors to identify aerospace objects. *IEEE Transactions on Antennas and Propagation*, 41(3):261–268, 1993.
- [10] Gilbert Strang. *Linear algebra and its applications*. Thomson, Brooks/Cole, Belmont, CA, 2006.
- [11] Tomas Mikolov, Ilya Sutskever, Kai Chen, Greg S Corrado, and Jeff Dean. Distributed representations of words and phrases and their compositionality. In C.J. Burges, L. Bottou, M. Welling, Z. Ghahramani, and K.Q. Weinberger, editors, *Advances in Neural Information Processing Systems*, volume 26. Curran Associates, Inc., 2013.
- [12] Chen Wang, Wenshan Wang, Yuheng Qiu, Yafei Hu, and Sebastian A. Scherer. Visual memorability for robotic interestingness via unsupervised online learning. *CoRR*, abs/2005.08829, 2020.
- [13] Chen Wang, Le Zhang, Lihua Xie, and Junsong Yuan. Kernel cross-correlator. *Proceedings of the AAAI Conference on Artificial Intelligence*, 32(1), Apr. 2018.
- [14] Zitong Yu, Xiaobai Li, Pichao Wang, and Guoying Zhao. Transrppg: Remote photoplethysmography transformer for 3d mask face presentation attack detection. *CoRR*, abs/2104.07419, 2021.
- [15] Elhanan Elboher and Michael Werman. Asymmetric correlation: A noise robust similarity measure for template matching. *IEEE Transactions on Image Processing*, 22(8):3062–3073, 2013.
- [16] J.P. Lewis. Fast normalized cross-correlation. *Ind. Light Magic*, 10, 10 2001.
- [17] Pentti Kanerva. Hyperdimensional computing: An introduction to computing in distributed representation with high-dimensional random vectors. *Cognitive Computation*, 1:139–159, 2009.
- [18] Anthony Thomas, Sanjoy Dasgupta, and Tajana Rosing. A theoretical perspective on hyperdimensional computing. *J. Artif. Int. Res.*, 72:215–249, jan 2022.
- [19] Mohamad H. Hassoun. *Associative neural memories : theory and implementation*. 1993.
- [20] Trenton Bricken and Cengiz Pehlevan. Attention approximates sparse distributed memory. In M. Ranzato, A. Beygelzimer, Y. Dauphin, P.S. Liang, and J. Wortman Vaughan, editors, *Advances in Neural Information Processing Systems*, volume 34, pages 15301–15315. Curran Associates, Inc., 2021.
- [21] Mohsen Imani, Zhuowen Zou, Samuel Bosch, Sanjay Anantha Rao, Sahand Salamat, Venkatesh Kumar, Yeseong Kim, and Tajana Rosing. Revisiting hyperdimensional learning for fpga and low-power architectures. In *2021 IEEE International Symposium on High-Performance Computer Architecture (HPCA)*, pages 221–234, Feb 2021.
- [22] Alejandro Hernández-Cano, Namiko Matsumoto, Eric Ping, and Mohsen Imani. Onlinehd: Robust, efficient, and single-pass online learning using hyperdimensional system. In *2021 Design, Automation And Test in Europe Conference and Exhibition (DATE)*, pages 56–61, 2021.
- [23] Karl Pearson. Note on regression and inheritance in the case of two parents. *Proceedings of the Royal Society of London*, 58:240–242, 1895.
- [24] Shantanu Chakrabartty and Gert Cauwenberghs. Margin propagation and forward decoding in analog VLSI. 2003.

- [25] Peter J. Huber. Robust Estimation of a Location Parameter. *The Annals of Mathematical Statistics*, 35(1):73 – 101, 1964.
- [26] Giuseppe C. Calafiore, Stephane Gaubert, and Corrado Possieri. A universal approximation result for difference of log-sum-exp neural networks. *IEEE Transactions on Neural Networks and Learning Systems*, 31(12):5603–5612, 2020.
- [27] Hanting Chen, Yunhe Wang, Chunjing Xu, Boxin Shi, Chao Xu, Qi Tian, and Chang Xu. Addernet: Do we really need multiplications in deep learning? *CVPR*, 2020.
- [28] Jr. Faran, James J. A simple electronic correlator. *The Journal of the Acoustical Society of America*, 24(4):452–452, 06 2005.
- [29] E. McMahon. An extension of price’s theorem (corresp.). *IEEE Transactions on Information Theory*, 10(2):168–168, 1964.
- [30] R. Price. A useful theorem for nonlinear devices having gaussian inputs. *IRE Transactions on Information Theory*, 4(2):69–72, 1958.
- [31] A. Papoulis. Comments on ‘an extension of price’s theorem’ by mcmahon, e. l. *IEEE Transactions on Information Theory*, 11(1):154–154, 1965.
- [32] Achim Klenke. *Probability Theory: A Comprehensive Course*. Springer, 2007.
- [33] C. adhakrishna Rao. Information and accuracy attainable in the estimation of statistical parameters. *Bulletin of the Calcutta Mathematical Society*, 37(3):81–91, 1945.
- [34] Rory A. Fisher. On the mathematical foundations of theoretical statistics. *Philosophical Transactions of the Royal Society A*, 222:309–368.
- [35] Ming Gu and Shantanu Chakrabartty. Synthesis of bias-scalable cmos analog computational circuits using margin propagation. *IEEE Transactions on Circuits and Systems I: Regular Papers*, 59(2):243–254, 2012.
- [36] Abhishek Ramdas Nair, Pallab Kumar Nath, Shantanu Chakrabartty, and Chetan Singh Thakur. Multiplierless mp-kernel machine for energy-efficient edge devices. *IEEE Transactions on Very Large Scale Integration (VLSI) Systems*, 30(11):1601–1614, 2022.